Axonal pathology in hPSC-based models of Parkinson's disease results from loss of Nrf2 transcriptional activity at the Map1b gene locus

Christopher Czaniecki[a,1], Tammy Ryan[a,1], Morgan G. Stykel[a], Jennifer Drolet[a], Juliane Heide[a], Ryan Hallam[a], Shalandra Wood[a], Carla Coackley[a], Keith Sherriff[a], Craig D. C. Bailey[b], and Scott D. Ryan[a,c,2]

[a]Department of Molecular and Cellular Biology, The University of Guelph, Guelph, ON, Canada N1G 2W1; [b]Department of Biomedical Sciences, The University of Guelph, Guelph, ON, Canada N1G 2W1; and [c]Neurodegenerative Disease Center, Scintillon Institute, San Diego, CA 92121

While mutations in the *SNCA* gene (α-synuclein [α-syn]) are causal in rare familial forms of Parkinson's disease (PD), the prevalence of α-syn aggregates in the cortices of sporadic disease cases emphasizes the need to understand the link between α-syn accumulation and disease pathogenesis. By employing a combination of human pluripotent stem cells (hPSCs) that harbor the *SNCA*-A53T mutation contrasted against isogenic controls, we evaluated the consequences of α-syn accumulation in human A9-type dopaminergic (DA) neurons (hNs). We show that the early accumulation of α-syn in *SNCA*-A53T hNs results in changes in gene expression consistent with the expression profile of the substantia nigra (SN) from PD patients, analyzed post mortem. Differentially expressed genes from both PD patient SN and *SNCA*-A53T hNs were associated with regulatory motifs transcriptionally activated by the antioxidant response pathway, particularly Nrf2 gene targets. Differentially expressed gene targets were also enriched for gene ontologies related to microtubule binding processes. We thus assessed the relationship between Nrf2-mediated gene expression and neuritic pathology in *SNCA*-A53T hNs. We show that *SNCA*-mutant hNs have deficits in neuritic length and complexity relative to isogenic controls as well as contorted axons with Tau-positive varicosities. Furthermore, we show that mutant α-syn fails to complex with protein kinase C (PKC), which, in turn, results in impaired activation of Nrf2. These neuritic defects result from impaired Nrf2 activity on antioxidant response elements (AREs) localized to a microtubule-associated protein (Map1b) gene enhancer and are rescued by forced expression of Map1b as well as by both Nrf2 overexpression and pharmaceutical activation in PD neurons.

human pluripotent stem cells | Parkinson's disease | α-synuclein | Nrf2 | Map1b

Parkinson's disease (PD) is characterized by a progressive decline in voluntary motor function that is caused by the death of A9-type dopaminergic (DA) neurons in the substantia nigra (SN). The loss of these neurons is preceded by the accumulation of intracellular proteinaceous aggregates, known as Lewy bodies and Lewy neurites, that contain an array of misfolded protein, primarily composed of α-synuclein (α-syn) (1). Accumulation of oligomeric species of α-syn has been implicated in both sporadic and familial cases of PD, including the A53T (G209A) mutation in the α-syn gene (*SNCA*-A53T), which is associated with early disease onset (2). Experimental models support a role for α-syn aggregation in degeneration of DA and other neuronal cell types. Transgenic overexpression of A53T-mutant α-syn in mice leads to neuronal dysfunction and behavioral impairments that parallel the formation of α-syn immunoreactive deposits in neurites of both cortical and midbrain neurons (3, 4). Ectopic exposure to α-syn preformed fibrils similarly induces widespread axonal neuropathology and subsequent neuronal death (5, 6). While *SNCA* mutations are causal in rare familial forms of PD and dramatically increase the risk of both motor and nonmotor disease symptoms (including dementia) (2, 7), the prevalence of α-syn aggregates in Lewy neurites found in the

brains of idiopathic disease cases emphasizes the need to understand how α-syn accumulation leads to axodendritic neuropathology.

The striatal axonal bush of a single DA neuron whose soma resides in the substantia nigra pars compacta (SNpc) can cover over 5% of the total volume of the neostriatum (8), indicating that nigrostriatal neurons are among the most highly arborized neurons in the brain. Indeed, neuropathological retraction of a single SN axon is estimated to influence upward of 75,000 striatal neurons (8). Lewy neurites sequester multiple proteins that are critical to axonal morphology and function. Tau is a microtubule-associated protein (MAP) of the MAP2 family, whereas Map1b is a microtubule lattice binding protein of the MAP1 class. Although both protein families are involved in microtubule stabilization, Tau is primarily located in the axons of healthy, mature neurons and maintains axon structure, while Map1b is prominently expressed during neuronal development and has been implicated in axodendritic growth and guidance (9, 10). Moreover, Tau has been identified as a major component of Lewy neurites, and Tau pathology has been described in familial cases of parkinsonism linked to *SNCA* mutations (11, 12). By contrast, Map1b has been reported in Lewy bodies of post mortem cortical isolates from patients with Lewy body dementia (13), suggesting that loss of

---

Significance

Neurological dysfunction in Parkinson's disease (PD) is highly associated with pathological deposits of aggregated α-synuclein (α-syn) in the brain, and yet an understanding of how early α-syn deposits bring about neuronal dysfunction remains elusive. This study exploits stem cell technology to model PD using two human isogenic stem cell models of the disease. Using these systems, we have identified a mechanism whereby mutant α-syn inhibits the antioxidant response, which, in turn, leads to axonal pathology through loss of expression of microtubule stabilizing proteins. We show that reactivation of this pathway can rescue axonal neuropathology. This is a demonstration of modulation of cytoskeletal elements as a potential therapy against PD, providing a previously unknown link between α-syn mutation and the antioxidant pathway.

---

function of microtubule stabilizing proteins may be linked to axonal pathology in multiple synucleinopathies.

To study the impact of α-syn accumulation on axodendritic pathology in human DA neurons (hNs), we employed a combination of human pluripotent stem cells (hPSCs). These consisted of 1) isogenic human embryonic stem cell (hESC)-derived neurons that were either wild type (WT) in origin or that had the SNCA-G209A mutation (A53T amino acid substitution) introduced through genome editing, as well as 2) isogenic human induced pluripotent stem cell (hiPSC)-derived neurons that either harbored an endogenous SNCA-G209A mutation or had this mutation reversed through genome editing (14, 15). Using these systems, we show that the early accumulation of α-syn in SNCA-A53T hNs results in differential gene expression consistent with the expression profile of PD patient SNpc analyzed post mortem. Differentially expressed genes from both PD patient SNpc and SNCA-A53T hNs were enriched for antioxidant response element (ARE) regulatory motifs and clustered to gene ontology (GO) terms related to microtubule binding processes and axonal projections. We therefore assessed the relationship between ARE activation by Nrf2, the primary effector of the antioxidant response, and axodendritic pathology in hiPSC- and hESC-derived SNCA-A53T hNs. We show that WT α-syn binds protein kinase C (PKC) and that α-syn mutation disrupts this binding in both hESC-derived and hiPSC-derived SNCA-A53T hNs, resulting in loss of phosphorylation and nuclear translocation of Nrf2, as well as loss of ARE activation. Furthermore, we show that SNCA-A53T hNs have deficits in both neurite length and complexity relative to isogenic controls and provide evidence that these neuritic defects result from impaired Nrf2 activity on AREs at the Map1b locus. Finally, we show that forced expression of Map1b by Nrf2 overexpression and pharmaceutical modulation of Nrf2 by dimethyl fumarate (DMF) rescues axodendritic deficits in PD neurons. This is a demonstration of Nrf2-mediated modulation of cytoskeletal elements as a potential therapy against PD.

Results

Human SNpc Tissue from PD Patients and SNCA-A53T hNs Share Common Transcriptional Deficits in the Antioxidant Response Pathway.
hPSC-derived hNs were terminally differentiated into tyrosine hydroxylase (TH)/DAT/DAP32 positive DA neurons by following a floor plate differentiation paradigm that routinely produces over 85% TH-positive neurons (15–17) (*SI Appendix*, Fig. S1 *A* and *B*), resulting in neurons with fast-spiking, tonic calcium transients (*SI Appendix*, Fig. S1*C*) characteristic of A9-type DA neurons. SNCA-A53T hNs of both hiPSC and hESC origin show increased α-syn phosphorylation at serine 129 (PS129) (*SI Appendix*, Fig. S1 *D–F*), which is predominantly present in detergent Triton-X 100-insoluble (*SI Appendix*, Fig. S1 *G* and *I*) and heat-stable (*SI Appendix*, Fig. S1 *H, J, and K*) deposits. To discern how synucleinopathy results in axonal neuropathology, we began by screening for biological processes that were consistently dysregulated in both hPSC-derived hNs and post mortem SNpc from PD patients, with a view to identifying molecular events that were altered early in disease progression (hPSC-derived hNs) and that remained altered throughout the disease (post mortem SNpc). We therefore contrasted the gene expression profiles of either hiPSC-derived or hESC-derived SNCA-A53T hNs with their isogenic controls. We performed a principal component (PC) analysis on the expression profiles of all cell lines to establish whether any observed variation in gene expression was due to line variation or the introduction/correction of the SNCA-A53T mutation (*SI Appendix*, Fig. S2*A*). PC1 separated all hESC samples from hiPSCs, but neither PC1 nor PC2 clustered samples in a manner dependent on the SNCA-A53T genotype. PC3, however, did separate samples in a genotype-dependent manner (*SI Appendix*, Fig. S2*A*), clustering

lines harboring the SNCA-A53T mutation from their isogenic counterparts. This suggests that the SNCA-A53T mutation has a similar effect on gene expression in neurons, regardless of whether the mutation is introduced by gene editing or is endogenously harbored.

We next correlated differentially expressed gene sets from hESC- and hiPSC-derived neurons with the gene expression profiles of post mortem human SN tissue from PD patients, contrasted against clinically normal control tissue. We found a total of 6,798 genes that were significantly changed between SNCA-A53T and control hNs, and 2,544 of these corresponded to genes that were differentially expressed between normal and PD SN tissue (Fig. 1 *A–C* and Dataset S1). Interestingly, the strongest correlation existed between genes down-regulated in both SNCA-A53T hNs and PD SN relative to their respective controls (Fig. 1*D*). A similarly strong correlation among down-regulated genes was observed when contrasting expression profiles of hESC-derived hNs harboring the SNCA-A53T mutation with PD SN (*SI Appendix*, Fig. S2*B* and Dataset S2). To group genes into functional categories, we first filtered differentially expressed gene sets based on regulatory motifs. Using the Molecular Signatures Database, we correlated differentially expressed genes with transcription factor binding motifs and identified several enriched response elements that clustered to down-regulated gene targets, including binding sites for ATF1, ATF2, ATF3, CREB, and Nrf2 (nuclear factor, erythroid 2-like 2 [NFE2L2]) (Fig. 1*E*). We next performed an enrichment analysis for canonical pathways using the GeneMania network prediction tool. Pathway analysis based on genes with binding motifs clustered to the above-noted transcription factors highlighted the antioxidant response pathway as a central hub for the regulation of the genes whose expression was lost in our dataset, with Nrf2 (NFE2L2) identified as the central modulator of down-regulated genes in this pathway (Fig. 1*F* and Dataset S3). Motif analysis of differentially expressed genes from hESC-derived SNCA-A53T hNs and PD SN also showed that ATF1, ATF2, ATF3, CREB, and Nrf2 binding motifs were enriched relative to controls (*SI Appendix*, Fig. S2*C* and Dataset S4). Finally, classification by GO revealed that differentially expressed genes within the antioxidant pathway clustered to GO terms relating to microtubule organization and neurite extension (Fig. 1*G* and *SI Appendix*, Fig. S2*D*). qPCR analysis confirmed that expression of genes clustered to the antioxidant pathway was lost in SNCA-A53T hNs of both hESC and hiPSC origin. Expression of phase i enzymes involved in the metabolic detoxification pathway and phase ii conjugation enzymes that metabolize functional groups (collectively referred to as phase i/ii detoxification enzymes) with putative or known Nrf2 binding motifs is decreased in SNCA-A53T hNs (Fig. 1*H*), as is expression of microtubule-associated genes with putative Nrf2 binding motifs (Fig. 1*I*). These data suggest that transcriptional activation of the antioxidant pathway is lost early in PD progression and remains inactive as the disease progresses. Moreover, the gene targets lost are critical for maintenance of axodendritic morphology and stability.

SNCA-A53T hNs Exhibit Deficits in Neurite Morphology.
Having determined that the expression of many genes involved in microtubule organization and axodendritic morphology was altered in PD relevant samples, we sought to examine neurite morphology in SNCA-mutant neurons, relative to their isogenic controls. We labeled both hiPSC-derived SNCA-A53T and corrected hNs (Fig. 2*A*) and hESC-derived WT and SNCA-A53T hNs (Fig. 2*G*) with antibodies directed to the dendritic marker MAP2 and the DA neuron marker, TH. We then performed Sholl analysis to quantify neuritic length and complexity. Results showed a significant global decrease in dendritic complexity of SNCA-A53T hNs relative to their respective isogenic controls in both hiPSC- and hESC-derived hNs (Fig. 2 *B*, *C*, *H*, and *I*). Moreover, both hiPSC-derived and hESC-derived SNCA-A53T hNs also showed a decrease in overall neurite

NEUROSCIENCE
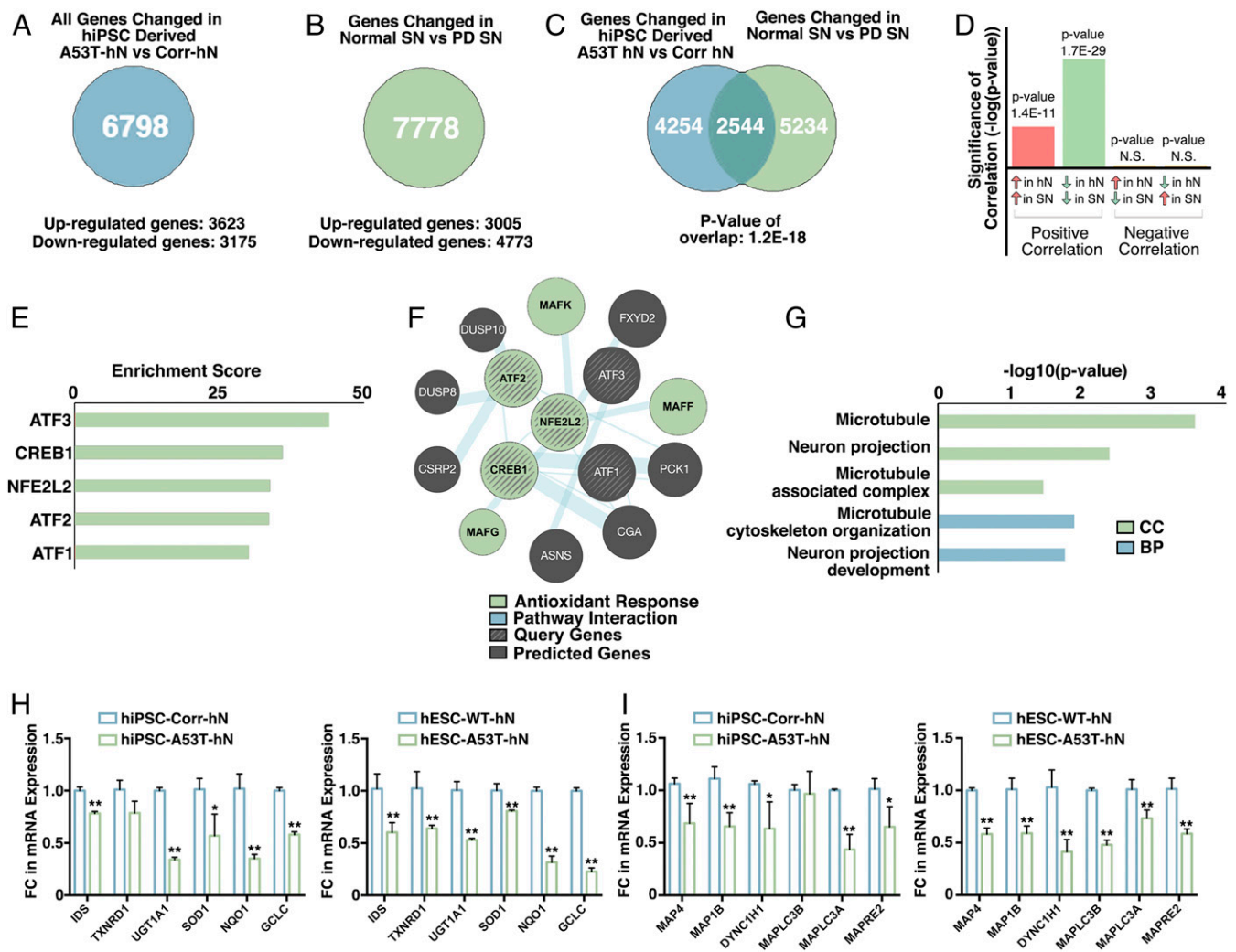
Fig. 1. Antioxidant response pathway is down-regulated in both *SNCA*-A53T hiPSCs and SNpc from PD patients. Expression profiles of genes significantly altered in *SNCA*-A53T hNs relative to *SNCA*-corrected hNs (*A*) were compared against the gene expression profile of SN from 8 PD patients (Braak α-syn stages 5 through 6) relative to 8 clinically normal controls (Braak α-syn stage 0) harvested post mortem (*B*) to identify differentially expressed genes present in both PD hNs and PD SN (*C*). (*D*) Changes in gene expression between PD hNs and PD SN were correlated for differentially expressed genes present in both gene sets. N.S., not significant. (*E*) All genes whose expression was statistically altered ($P < 0.05$, Fisher exact test) by at least 1-fold in A53T relative to corrected hNs or in PD SN relative to clinically normal SN were filtered based on regulatory motifs using Illumina's BaseSpace Correlation Engine (46), and the most enriched regulatory motifs and their associated enrichment scores are depicted. (*F*) To determine whether the identified transcriptional regulators are associated with a common cellular pathway, a network analysis was performed in GeneMania using the identified transcription factors as the query, and the resulting network was weighted based on molecular function. To group differentially expressed genes associated with the identified transcription factors into functional categories, the associated differentially expressed genes within both *SNCA*-A53T hNs and PD SNpc were clustered for GO terms using the Database for Annotation, Visualization and Integrated Discovery (DAVID) v6.7. The cutoff for the level of significance over background was $P < 0.05$ using Fisher's exact test with correction for multiple hypothesis testing by the algorithm of Benjamini and Hochberg. The background set of genes used was the entire human genome. (*G*) Most significant GO terms are depicted. BP, biological process; CC, cellular compartment. qPCR analysis of expression of genes with putative Nrf2 binding motifs that function in either phase i/ii enzyme detoxification (*H*) or microtubule function (*I*) in both hiPSC- and hESC-derived hNs is illustrated. FC, fold change; mRNA, messenger RNA. Data represent mean ± SEM. *$P < 0.05$; **$P < 0.01$ by multiple analysis of variance (MANOVA) and post hoc Tukey test ($n = 3$ independent differentiations).

length (Fig. 2 *D* and *J*) relative to their isogenic controls, implying early evidence of impaired axodendritic function. We next sought to determine if this correlated with axonal neuropathology. We labeled hiPSC-derived (Fig. 2 *E* and *F*) and hESC-derived (Fig. 2 *K* and *L*) hNs for Tau and examined axons for pathological features previously reported in animal models and in the brains of PD patients harboring the *SNCA*-A53T mutation, including contorted or fragmented axons with swollen Tau-positive varicosities (12, 18, 19). Indeed, *SNCA*-A53T hNs exhibited greater numbers of Tau-labeled varicosities than their isogenic counterparts (Fig. 2 *E*, *F*, *K*, and *L*). Collectively, these results show that the *SNCA*-A53T mutation results in defects in axodendritic morphology and Tau

neuropathology in hPSC-derived hNs that are consistent with those seen in PD patient samples.

SNCA-A53T hNs Exhibit Deficits in ARE Activity Coupled to Increased Oxidative Stress. We next sought to assess the consequences of loss of phase i/ii detoxifying enzyme expression in *SNCA*-A53T hNs and to determine whether the loss of ARE activation was the reason for this deficit. We first labeled hiPSC-derived *SNCA*-A53T and corrected hNs with MitoSOX to measure superoxide anion production. We found *SNCA*-A53T hNs displayed increased superoxide anion production (Fig. 3 *A* and *B*), and this correlated with a decrease in basal ARE activity in *SNCA*-A53T hNs (Fig. 3*C*). Cotransformation with both ARE-driven luciferase and a

Czaniecki et al.
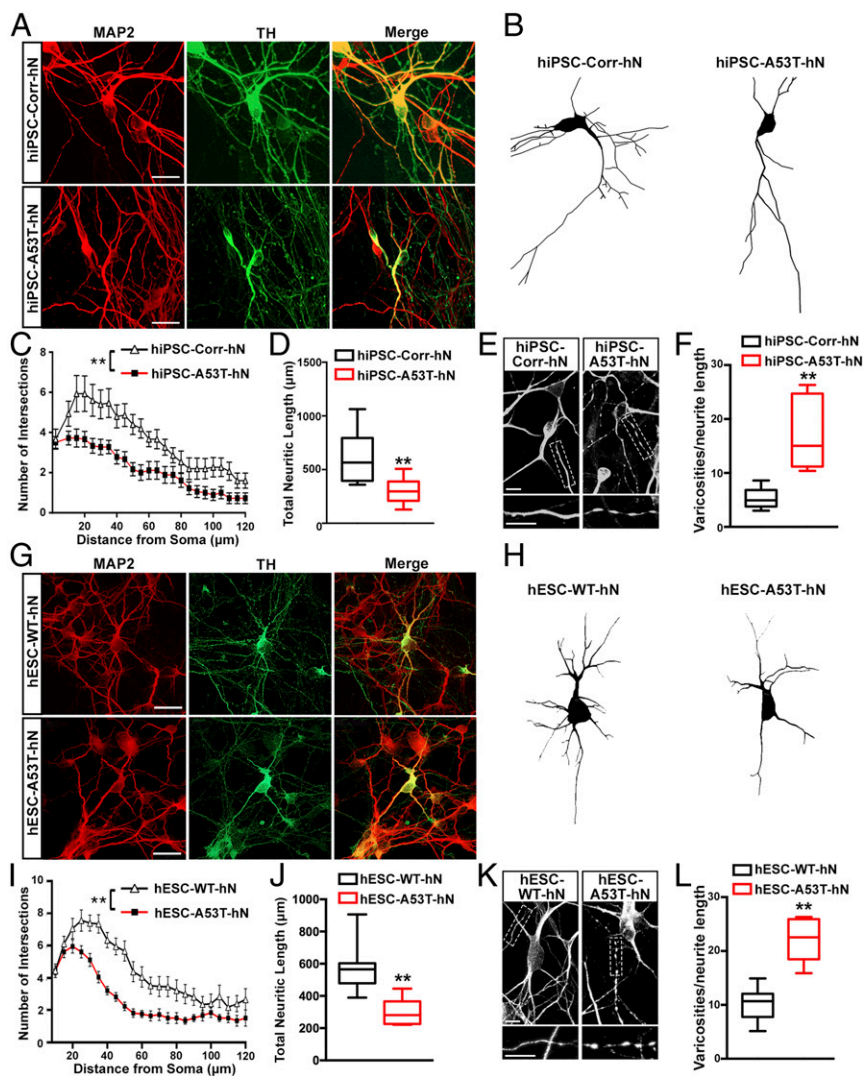
Fig. 2. *SNCA* mutation results in axonal pathology. Axodendritic pathology was assessed in hiPSC-derived *SNCA*-A53T and corrected (Corr) hNs (*A–F*) or hESC-derived WT and *SNCA*-A53T hNs (*G–L*). The hiPSC-derived (*A*) and hESC-derived (*G*) hNs were labeled with antibodies against MAP2 and TH, and were subsequently traced using Neurolucida (*B* and *H*). (Scale bars: 10 μm.) The example traces depicted (*B* and *H*) are the same neurons labeled for TH (*A* and *G*). The orientation of the trace was adjusted for ease of comparison. A Sholl analysis showed that both hiPSC- and hESC-derived *SNCA*-A53T hNs have less complex neuritic networks (*C* and *I*) and a shorter average neurite length (*D* and *J*) than their respective controls. **$P < 0.01$ by multiple analysis of variance (MANOVA) and post hoc Tukey test (*C* and *I*) or *t* test (*D* and *J*) ($n = 70$ to 78 individual neurons). The hiPSC-derived (*E* and *F*) and hESC-derived (*K* and *L*) hNs were labeled with antibodies against Tau, and the number of axonal varicosities per neurite length were measured. (Scale bars: 10 μm.) **$P < 0.01$ by *t* test ($n = 20$ individual neurons).

constitutively active Renilla permitted normalization of luminescence between lines and showed that basal ARE activation in *SNCA*-A53T hNs is significantly lower than in control neurons (Fig. 3*C*). To determine whether pharmacological activation of Nrf2 activation could rescue phase i/ii detoxifying enzyme expression in PD neurons, we treated *SNCA*-WT and *SNCA*-A53T hNs with DMF, a known activator of Nrf2 (20). DMF is in clinical use for multiple sclerosis, under the trade name Tecfidera (21). DMF treatment results in S-alkylation of Keap1, which destabilizes the Keap1/Nrf2 complex, preventing Nrf2 degradation and permitting Nrf2 nuclear translocation, thereby activating the antioxidant response (20). Interestingly, we found that DMF induced ARE activity in both *SNCA*-WT and *SNCA*-A53T hNs (Fig. 3*C*). Indeed, when hNs overexpressing Nrf2 were treated with DMF, there was an additive effect with respect to ARE reporter activation, supporting the previous reports that DMF activation of the ARE is mediated through Nrf2 (*SI Appendix*, Fig. S3*A*). Having validated DMF as an effective pharmacological agent for activation of Nrf2 in *SNCA*-A53T hNs, we assessed the effect of Nrf2 activation on phase i/ii detoxifying enzymes. DMF treatment rescued expression of multiple phase i/ii detoxifying enzymes in both hiPSC-derived (Fig. 3 *D* and *E* and *SI Appendix*, Fig. S3*B*) and hESC-derived (Fig. 3 *F* and *G* and *SI Appendix*, Fig. S3*B*) *SNCA*-A53T hNs. This effect was most prominent for the enzymes NAD(P)H quinone dehydrogenase 1, a major quinone reductase in neurons,

and glutamate–cysteine ligase catalytic subunit (GCLC), the first and a rate-limiting step in the synthesis of glutathione, which are critical components of the antioxidant response (22).

The Subcellular Localization of Nrf2 Is Disrupted in *SNCA*-A53T hNs. To better understand the reason for the deficit in Nrf2 activation on *SNCA*-A53T hNs, we next assessed Nrf2 localization and phosphoactivation. Under basal conditions, Nrf2 transcriptional activity is inhibited by its association with Keap1, which promotes ubiquitylation and degradation of Nrf2 protein (23). Under conditions of oxidative stress, cysteine oxidation of Keap1 results in dissociation of this complex, stabilizing Nrf2 and permitting translocation of Nrf2 to the nucleus, where it binds AREs and activates the expression of genes involved in the antioxidant response. In addition to redox-mediated dissociation of Nrf2 from Keap1, phosphorylation of Nrf2 at serine 40 by PKC has been reported to directly inhibit Keap1/Nrf2 binding (24, 25). To further understand the link between the antioxidant response pathway and neurite pathology in our system, we next sought to investigate the phosphorylation status and subcellular localization of Nrf2. Whereas there was no significant difference in the levels of total Nrf2 between *SNCA*-A53T hNs and their isogenic control lines in either hESC-derived or hiPSC-derived neurons, there was a significant decrease in the levels of Nrf2-PSer40 in *SNCA*-A53T hNs relative to isogenic control lines (Fig. 4 *A* and *B*).

Czaniecki et al.
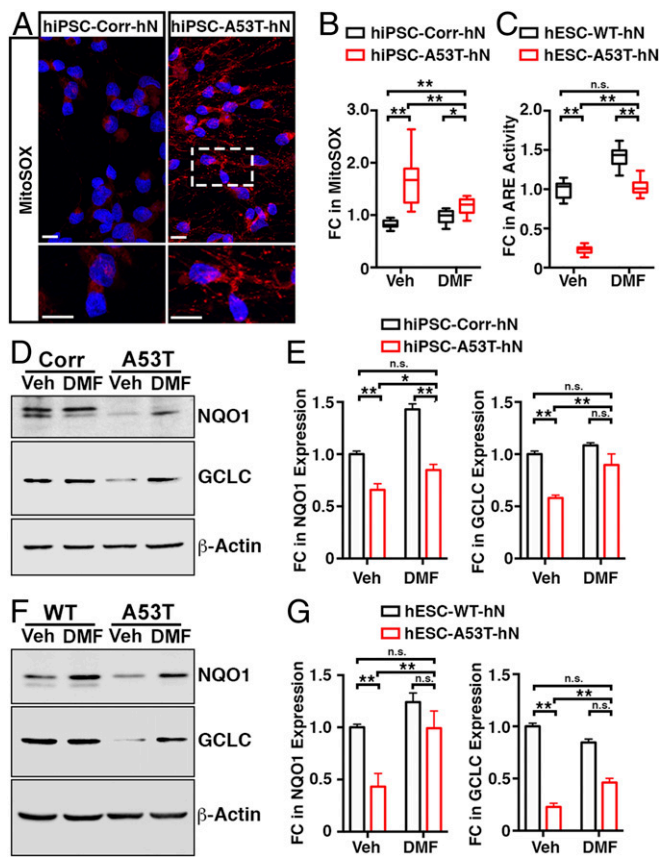
Fig. 3. *SNCA*-A53T hNs exhibit deficits in ARE activity coupled to increased oxidative stress. (*A* and *B*) MitoSOX labeled *SNCA*-A53T hNs show increased superoxide anion levels that are rescued by DMF treatment. (Scale bars: 10 μm). **$P < 0.01$ by multiple analysis of variance (MANOVA) and post hoc Tukey test ($n = 24$ coverslips). Corr, corrected; FC, fold change; Veh, vehicle. (*C*) Nrf2 transcriptional activity was assessed in *SNCA*-A53T and control hNs by luciferase assay using an ARE-Luc reporter construct in the presence and absence of DMF. **$P < 0.01$ by MANOVA and post hoc Tukey test ($n = 6$ coverslips). n.s., not significant. Western blot analysis of Nrf2 target expression in hiPSC-derived (*D* and *E*) and hESC-derived (*F* and *G*) hNs in the presence and absence of DMF is illustrated. Data represent mean $\pm$ SEM. **$P < 0.01$ by MANOVA and post hoc Tukey test ($n = 3$ independent differentiations).

We next performed subcellular fractionations of hESC-derived *SNCA*-WT and *SNCA*-A53T hNs to assess the localization of Nrf2. We performed Western blots of input, cytoplasmic, and nuclear fractions using βIII-tubulin and histone H3 as markers of the cytoplasmic and nuclear fractions, respectively (Fig. 4*C*). Consistent with the decreased levels of Nrf2-PSer40, there was significantly less Nrf2 in nuclear fractions isolated from *SNCA*-A53T hNs relative to *SNCA*-WT nuclei. This coincided with the accumulation of α-syn protein in detergent-insoluble, heat-stable deposits (*SI Appendix*, Fig. S1 *F* and *G*) and increased baseline oxidative stress (Fig. 3 *A* and *B*) in *SNCA*-A53T.

PKC is reported to phosphorylate Nrf2 at Ser40, leading to dissociation of the Nrf2/Keap1 complex and nuclear translocation of Nrf2 (25). Given previously published reports that have suggested α-syn can interact with PKC by acting as a 14-3-3–like adaptor protein, bringing PKC into close proximity with its substrates (26), we hypothesized that α-syn mutation and subsequent deposition into insoluble aggregates might disrupt this interaction, leading to the loss of Nrf2 phosphorylation. We thus performed α-syn immunoprecipitation from both hESC-derived (Fig. 4*D*) and hiPSC-derived (*SI Appendix*, Fig. S4*A*) *SNCA*-A53T hNs and assessed the levels of bound PKC relative to

isogenic controls. Indeed, both PKC and Nrf2 were detected on immunoprecipitation of α-syn from control hNs, but binding to both proteins was dramatically reduced in *SNCA*-A53T neurons. These data suggest that α-syn does indeed act as an adaptor protein, bridging PKC and Nrf2, thereby facilitating Nrf2 activation. To test this hypothesis, we used the PKC activator bryostatin to drive PKC activity in both control and *SNCA*-A53T hNs. If α-syn disrupts a functionally relevant interaction between PKC and Nrf2, then PKC activation by bryostatin would induce Nrf2 phosphorylation and subsequent ARE activation in control
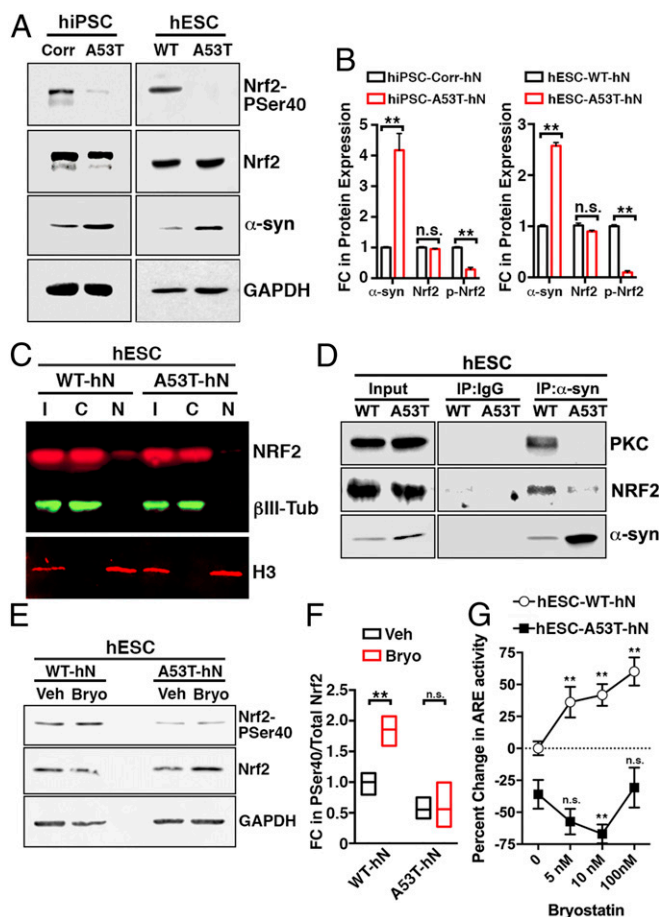
Fig. 4. α-Syn is required for activation of Nrf2 by PKC. (*A* and *B*) Western blot analysis of lysates from hiPSC- and hESC-derived neurons probed for total α-syn, Nrf2, Nrf2-Phospho-serine 40, or glyceraldehyde-3-phosphate dehydrogenase (GAPDH) shows that *SNCA*-A53T hNs have lower levels of Nrf2-Phospho-serine 40. Data represent mean $\pm$ SEM. **$P < 0.01$ by t test ($n = 3$ independent differentiations). Corr, corrected; FC, fold change; n.s., not significant. (*C*) hNs were subjected to nuclear versus cytosolic fractionation, and protein was analyzed by Western blot. βIII-tubulin (βIII-Tub) and histone H3 were used as markers of cytoplasmic and nuclear fractions, respectively. A53T hNs exhibit lower levels of nuclear Nrf2 relative to WT hNs. C, cytoplasmic; I, input; N, nuclear. (*D*) α-Syn or IgG was immunoprecipitated from *SNCA*-A53T and WT lysates. Subsequent Western blot analysis for α-syn, Nrf2, and PKC shows that in WT neurons, α-syn binds Nrf2 and PKC, while in *SNCA*-A53T neurons, binding to α-syn is inhibited. (*E* and *F*) Western blot analysis of lysates from hESC-derived neurons probed for total Nrf2, Nrf2-Phospho-serine 40, or GAPDH following treatment with the PKC agonist bryostatin (Bryo). Data represent mean $\pm$ SEM. **$P < 0.01$ by t test ($n = 3$ independent differentiations). (*G*) Nrf2 transcriptional activity was assessed in *SNCA*-A53T and control hNs by luciferase assay using an ARE-Luc reporter construct in the presence and absence of bryostatin. **$P < 0.01$ by ANOVA and post hoc Dunnett test against respective 0 nM controls ($n = 6$ independent differentiations).

hNs but not in *SNCA*-A53T hNs. As predicted, we found that bryostatin induces Nrf2 phosphorylation (Fig. 4 *E* and *F*) and ARE reporter activation (Fig. 4*G*) in *SNCA*-WT hNs but not in *SNCA*-A53T hNs. Collectively, this suggests that mutation of α-syn inhibits activation of the antioxidant response by disrupting α-syn interaction with PKC, resulting in impaired phosphorylation of Nrf2 and inhibition of Nrf2 nuclear translocation.
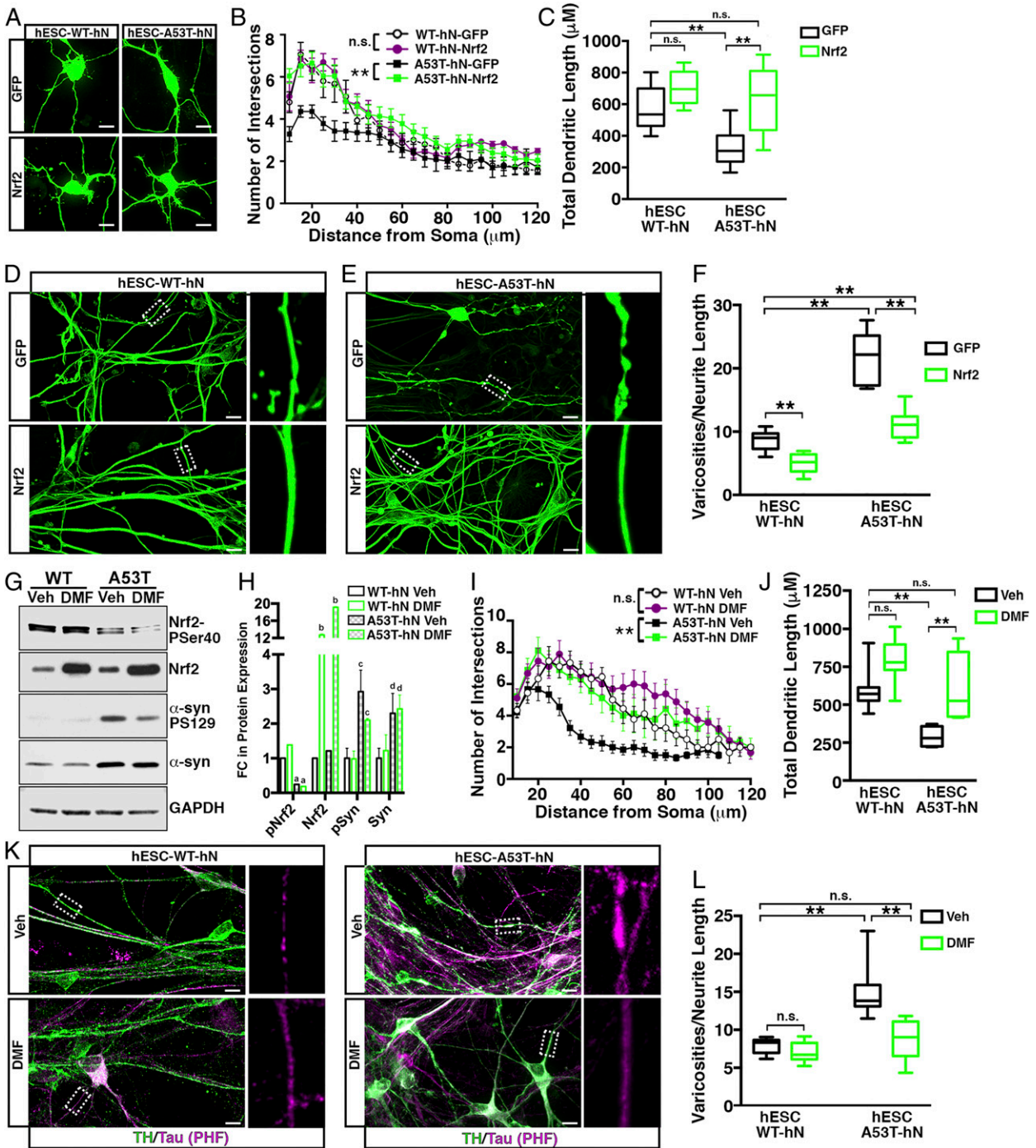
Forced Activation of the Antioxidant Response Rescues Neuritic Defects in *SNCA*-A53T Neurons. Our bioinformatic analysis of transcription factor binding motifs down-regulated in PD suggests that deficits in neuritic length and complexity in A53T hNs may be linked to impairments in the antioxidant response. To test this directly, we activated the antioxidant response by overexpressing Nrf2 and reassessed axodendritic pathology. Overexpression of Nrf2 in neurons overwhelms the Keap1 degradation machinery and leads to stabilization of Nrf2 protein (27). We thus overexpressed Nrf2 or a GFP control in *SNCA*-A53T and *SNCA*-WT hNs (Fig. 5 *A*–*G*). Overexpression of Nrf2 in *SNCA*-A53T hNs rescued both neuritic complexity (Fig. 5*B*) and total dendritic length (Fig. 5*C*). To determine if Nrf2 expression also rescued axonal neuropathology, we reassessed axonal varicosities in hESC-derived hNs overexpressing either GFP or Nrf2. Indeed, the increased number of varicosities previously observed in *SNCA*-A53T hNs was significantly reduced in Nrf2-overexpressing neurons (Fig. 5 *D*–*F*), suggesting that forced activation of the Nrf2 pathway rescues axonal pathology previously reported both in the brains of PD patients and in hiPSC-derived hNs (12, 18, 28).

To determine whether a pharmacological approach to Nrf2 activation could similarly rescue axodendritic pathology in PD neurons, we again treated *SNCA*-WT and *SNCA*-A53T hNs with the Nrf2 activator DMF (20). We first confirmed the effect of DMF treatment on Nrf2 degradation by measuring Nrf2 protein levels and found DMF effectively blocked Nrf2 degradation in both *SNCA*-A53T and control neurons (Fig. 5 *G* and *H*). No effect on Nrf2 phosphorylation was observed following DMF treatment (Fig. 5 *G* and *H*), consistent with previous reports that DMF acts primarily by promoting Nrf2 stability (20). Similarly, no significant effect on either total or PS129-modified α-syn levels was observed following DMF treatment (Fig. 5 *G* and *H*). We next assessed the effect of DMF-mediated Nrf2 activation on axodendritic pathology. A Sholl analysis of *SNCA*-WT and *SNCA*-A53T hNs treated with DMF showed DMF rescued both neuritic complexity (Fig. 5*I*) and total neurite length (Fig. 5*J*), such that there was no significant difference between DMF-treated *SNCA*-A53T hNs and their isogenic WT counterparts. Finally, we labeled DMF-treated control and *SNCA*-A53T hNs for hyperphosphorylated Tau and examined axons for pathological features. *SNCA*-A53T hNs exhibited greater numbers of Tau-labeled varicosities than isogenic controls (Fig. 5 *K* and *L*), and these were significantly reduced by DMF treatment. These data provide direct evidence of a role for the antioxidant response pathway and, more specifically, for Nrf2 activity in the maintenance of neurite integrity.

Map1b Is a Nrf2 Transcriptional Target Whose Expression Regulates Axodendritic Pathology in PD. We have shown *SNCA*-A53T hNs have neuritic deficits relative to their WT counterparts and that this is due, at least in part, to decreased Nrf2 activity and, consequently, loss of expression of antioxidant response genes. Our GO analysis identified genes associated with the microtubule as a prominent cluster in *SNCA*-A53T hNs and PD SNpc tissue (Fig. 6*A*). We therefore assessed genes in this category that were down-regulated in both *SNCA*-A53T hNs and PD SNpc and have been attributed a role in axodendritic projection for their responsiveness to DMF (*SI Appendix*, Fig. S5 *A–C*). The most consistent and significant change in expression upon DMF treatment was observed for Map1b (Fig. 6*B* and *SI Appendix*, Fig. S5*A*). Map1b is known to be an important regulator of both axonal and dendritic growth and guidance (29), while Tau is restricted to axons (10), and increased Tau expression is commonly associated with PD pathology (11, 12). *Mapt* is a known target of Nrf2 (30) and was therefore an attractive candidate, but confirmation of the expression profile results by qPCR indicated no significant difference in expression between hiPSC-derived (*SI Appendix*, Fig. S5*B*) and hESC-derived (*SI Appendix*, Fig. S5*C*) *SNCA*-A53T hNs relative to their isogenic controls. Moreover, DMF treatment did not affect *Mapt* expression in either system (*SI Appendix*, Fig. S5 *B* and *C*). Analysis of Map1b expression by qPCR, however, confirmed a significant decrease in *Map1b* messenger RNA levels in both hiPSC- and hESC-derived *SNCA*-A53T hNs relative to their isogenic controls (Figs. 1*I* and 6*B*). We therefore hypothesized that Map1b is a key transcriptional target of Nrf2, whose expression is critically associated with DMF-mediated rescue of the axodendritic pathologies observed in *SNCA*-A53T hNs. To assess this, we analyzed the *Map1b* locus for possible regulatory elements that could link *Map1b* expression to the antioxidant pathway by searching for putative ARE consensus sites. Our analysis focused on the *Map1b* promoter (31) as well as on a putative enhancer identified by ENCODE that spans the promoter, transcriptional start site (TSS), first exon, and 5′ region of the first intron (Fig. 6*C*). We identified three putative AREs within this enhancer. To confirm these were, in fact, Nrf2 binding sites, we performed chromatin immunoprecipitation (ChIP) in a neuronal context using an antibody against Nrf2. Since two of the AREs identified were in close proximity (90 bp apart, 3 kb downstream from the TSS), this region was treated as a single binding site for downstream analysis, while the third ARE was analyzed independently (4 kb downstream from the TSS). We found that Nrf2 was indeed recruited to the more proximal AREs following treatment with DMF (Fig. 6*D*). Moreover, the level of Nrf2 recruitment to the Map1b ARE was similar to that of a previously identified ARE in the GCLC locus (32, 33) (Fig. 6*D*), which served as a positive control. Nrf2 did not bind the third, more distal ARE, and it did not bind to an upstream negative control region devoid of an ARE consensus site. Finally, to show directly that loss of Nrf2 activity results in loss of *Map1b* gene expression, we silenced *NFE2L2* (Nrf2 gene) in a neural context (Fig. 6 *E*, *Inset*) and measured the effect on *Map1b* gene expression (Fig. 6*E*). As expected, the levels of *Map1b* expression were dramatically reduced in *shNFE2L2* cells relative to short hairpin RNA-scrambled controls, supporting a role for Nrf2 in transcriptional regulation of *Map1b* expression.

In our final set of experiments, we sought to determine whether restored expression of *Map1b* mechanistically explained the ability of DMF to rescue axodendritic pathology in *SNCA*-A53T hNs. We therefore overexpressed Map1b-GFP in these cells and repeated the Sholl analysis. Indeed, Map1b overexpression rescued both neurite length and complexity (Fig. 7 *A*–*C*). To determine if Map1b expression also rescues axonal neuropathology, we labeled hiPSC-derived hNs for Tau and measured the accumulation of Tau-positive varicosities. The increase in the number of varicosities previously observed in *SNCA*-A53T hNs was significantly reduced following Map1b overexpression in hiPSC-derived (Fig. 7*D*) and hESC-derived (Fig. 7*E*) *SNCA*-A53T hNs, suggesting that restored *Map1b* expression rescues the pathological features previously reported in the brains of both PD animal models and patients. Taken together, our results show that *Map1b* expression is regulated by Nrf2 via binding at an ARE within the first intron of the gene, providing a direct link between the antioxidant response pathway and maintenance of neurite length and complexity. Moreover, our findings suggest that *Map1b* expression is lost in both PD SN and *SNCA*-A53T neurons and that forced expression of Map1b rescues axodendritic pathology observed in these cells.

NEUROSCIENCE

www.manaraa.com

Fig. 5. Forced activation of the antioxidant response rescues neuritic defects in *SNCA*-A53T neurons. (*A*) Nrf2-GFP or GFP alone was transfected into *SNCA*-WT and *SNCA*-A53T hESC-derived hNs, and axodendritic pathology was assessed. (Scale bars: 10 μm.) (*B*) Sholl analysis showed that neuritic complexity was rescued by forced NRF2 expression. Statistical analysis was performed using the area under the curve. Data represent mean ± SEM. **$P < 0.01$ by multiple analysis of variance (MANOVA) and post hoc Tukey test ($n = 50$ individual neurons). n.s., not significant. (*C*) Sholl analysis of total neurite length. **$P < 0.01$ by MANOVA and post hoc Tukey test ($n = 50$ individual neurons). hNs from *SNCA*-WT (*D*) and *SNCA*-A53T (*E*) hESCs overexpressing Nrf2 or GFP were assessed for axonal varicosities. (Scale bars: 10 μm.) (*F*) Number of varicosities per neurite length was quantified. **$P < 0.01$ by MANOVA and post hoc Tukey test ($n = 20$ individual neurons). (*G*) Western blot analysis of lysates from hESC-derived neurons treated with either dimethyl sulfoxide (DMSO) or DMF were probed for total Nrf2, Nrf2-Phospho-serine 40, total α-syn, α-syn-Phospho-serine 129, or glyceraldehyde-3-phosphate dehydrogenase (GAPDH). Veh, vehicle. (*H*) Probed lysates were quantified. The y-axis break from 4 to 12 permits visualization of pNrf2 relative to total Nrf2. FC, fold change. Data represent mean ± SEM. a, b, c, d = $P < 0.01$ by ANOVA and post hoc Dunnett test against respective WT-hN vehicle for each protein assessed (a = pNrf2, b = Nrf2, c = pSyn, d = syn) ($n = 3$ independent differentiations). (*I*) Sholl analysis of *SNCA*-A53T and *SNCA*-WT hNs treated with DMSO (vehicle) or DMF showed that neuritic complexity was rescued by DMF treatment. Statistical analysis was performed using the area under the curve. Data represent mean ± SEM. **$P < 0.01$ by MANOVA and post hoc Tukey test ($n = 50$ individual neurons). (*J*) Sholl analysis of total neurite length following DMF treatment. **$P < 0.01$ by MANOVA and post hoc Tukey test ($n = 50$ individual neurons). (*K*) *SNCA*-A53T and control hNs treated with DMF were assessed for Tau-PHF–positive axonal varicosities per neurite length. (Scale bars: 10 μm.) (*L*) Quantification of Tau-positive varicosities per neurite length is presented. **$P < 0.01$ by MANOVA and post hoc Tukey test ($n = 20$ individual neurons).

www.manaraa.com
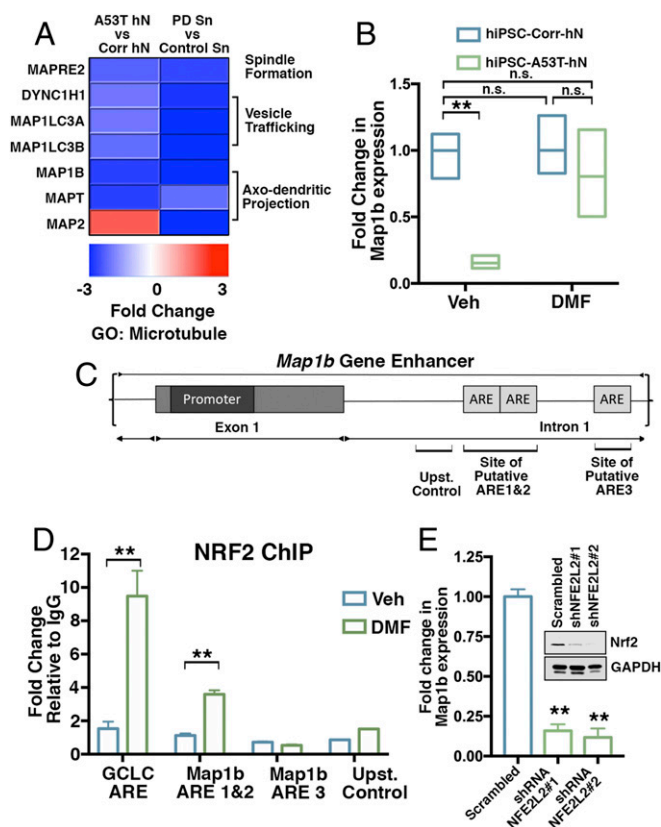
Fig. 6. Map1b is a Nrf2 transcriptional target whose expression is lost in PD. (*A*) Differentially expressed genes within both *SNCA*-A53T hNs and PD SN were clustered for GO terms as described in Fig. 1*F*. After clustering, genes associated with the Microtubule GO-Term were retained and fold changes were visualized using Morpheus (Broad Institute). Corr, corrected. (*B*) qRT-PCR analysis of *Map1b* expression in hiPSC-derived hNs following DMF treatment. **$P < 0.01$ by t test ($n = 3$ independent differentiations). n.s., not significant; Veh, vehicle. (*C*) *Map1b* promoter, TSS, and first intronic region were identified using UCSC Genome Browser, and these regions were screened for putative AREs using Multiple Sequence Local Alignment and Visualization (MULAN). Identified (putative) AREs clustered within Map1b Gene Enhancer and a representative schematic are depicted. Upst., upstream. (*D*) ChIP was performed using an antibody against Nrf2 and an isotype-specific IgG as a negative control. A known ARE regulating GCLC expression and an upstream genomic region devoid of AREs were used as positive and negative controls, respectively. Data represent mean ± SEM. **$P < 0.01$ by multiple analysis of variance (MANOVA) and post hoc Tukey test ($n = 3$ independent differentiations). (*E*) Differentiated neuronal cells were lentivirally transformed with short hairpin RNA (shRNA) against *NFE2L2* (Nrf2 gene) or scramble control. (*Inset*) Western blot analysis of Nrf2 protein levels was performed to confirm knockdown. qRT-PCR analysis of *Map1b* expression showed that shNFE2L2-transformed neurons had reduced *Map1b* expression. Data represent mean ± SEM. **$P < 0.01$ by ANOVA and post hoc Dunnett test ($n = 3$ independent differentiations).

Discussion

Oxidative stress occurring as a result of dopamine metabolism, mitochondrial dysfunction, and astrogliosis has been implicated in the death of DA neurons in PD (34). It has remained unclear, however, how sensitivity to oxidative stress is related to accumulation of insoluble α-syn aggregates, which are commonly associated with both idiopathic and familial cases of PD. Previous studies have focused primarily on the relationship between α-syn and mitochondrial dysfunction. We have previously shown that accumulation of α-syn oligomers promotes mitochondrial fragmentation (17), while others have found that α-syn oligomers disrupt calcium homeostasis, which also contributes to mitochondrial dysfunction

(35–37). Our gene expression analysis of post mortem SN from PD patient tissue and neurons derived from PD patient hiPSCs has identified the antioxidant response pathway as a key hub of differential gene expression between healthy and diseased cells. We show here that activation of the antioxidant response is directly inhibited by mutation of α-syn, specifically by disrupting its interaction with PKC, which, in turn, prevents phosphorylation and nuclear translocation of Nrf2. Moreover, our findings indicate that aberrant accumulation of α-syn exacerbates the sensitivity of DA neurons to oxidative stress, not only by promoting mitochondrial dysfunction but, in parallel, by interfering with the Nrf2-mediated antioxidant response. We find this loss of function to correlate highly with accumulation of α-syn into insoluble aggregates. As such, we would predict that other synucleinopathy-related genome alterations such as *SNCA*-A30P, *SNCA*-E46K, and gene duplication or triplication would also result in loss of Nrf2 activity, as those mutations similarly promote synuclein deposition into insoluble aggregates (38, 39).

Several reports have now shown that hPSC models of PD faithfully recapitulate neuropathology seen in human PD brains, including accumulation of α-syn and reduced neurite length (15, 28, 40). In this study, we show that deficits in neurite length occur, at least in part, as a result of decreases in the expression level of Map1b. Importantly, we have established a direct link between neurite integrity and the antioxidant response by identifying Map1b as a direct target of Nrf2, the master regulator of this pathway. The role of Map1b in PD is not fully understood; however, it has been shown to interact with α-syn as a component of Lewy bodies (13) and is also a target for DJ-1 chaperone activity (41). Conversely, it has also been shown to bind leucine-rich repeat kinase 2 (LRRK2) and inhibits its activity. When coexpressed with mutant LRRK2, Map1b rescued LRRK2-mediated toxicity in a neuroblastoma cell line (42). In our hPSC model, overexpression of Map1b or activation of its expression by treatment with the Nrf2 activator DMF resulted in rescue of neurite length deficits in A53T hNs. A recent study reported the *Mapt* gene is also regulated by binding of Nrf2 to an ARE within its first intron and that a single-nucleotide polymorphism associated with stronger Nrf2 binding results in increased expression of Tau protein and reduced risk of parkinsonian disorders (30). We examined *Mapt* in our system and found that gene expression was not significantly affected by the *SNCA*-A53T mutation, and its expression was not induced by treatment with the Nrf2 activator DMF. This discrepancy may suggest a difference in chromatin accessibility between classes of neurons, as the ChIP-sequencing data that identified *Mapt* as a Nrf2 transcriptional target were not obtained from DA neurons. Nevertheless, it is clear there is interplay between MAP expression and the antioxidant response, and that this interaction merits additional study in light of the fundamental role played by both of these factors in the pathogenesis of PD.

DMF is a Nrf2-activating compound with a history of safe use in the treatment of multiple sclerosis and psoriasis under the trade name Tecfidera (21, 43). DMF treatment results in S-alkylation of Keap1, which destabilizes the Keap1/Nrf2 complex (20). DMF also promotes nuclear export of the Nrf2 antagonist Bach1 (44). These two parallel processes result in increased Nrf2-mediated transcription of genes required for the antioxidant response. Given the contribution of oxidative stress to the pathogenesis of PD, there has been recent interest in the repurposing of DMF as a therapeutic agent for PD. Indeed, preclinical data indicate that it may hold promise in this role. Recent studies have shown that DMF protects against 1-methyl-4-phenyl-1,2,3,6-tetrahydropyridine, 6-hydroxydopamine, and α-syn toxicities in mice (44–47). Importantly, all of these studies demonstrated that Nrf2 was required for the therapeutic effects of DMF. Our study shows that treatment with DMF rescues axonal pathologies associated with PD in patient-derived hNs. Our

Czaniecki et al.

NEUROSCIENCE

www.manaraa.com
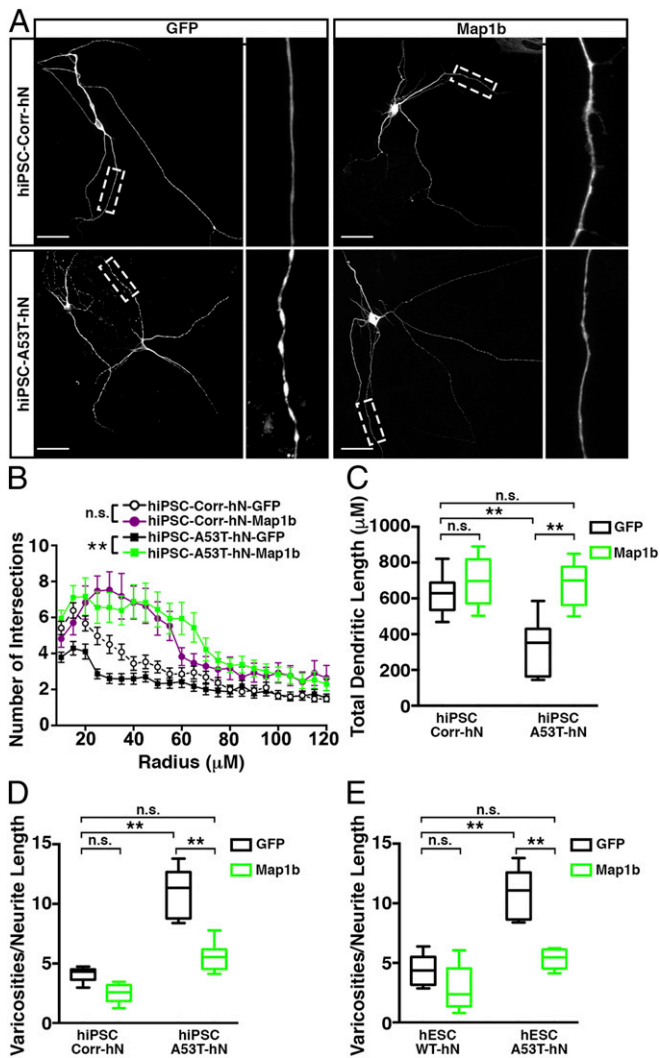
Fig. 7. Increasing Map1b expression rescues axodendritic pathology in PD. (*A–E*) Map1b-GFP or GFP alone was transfected into *SNCA*-A53T and control hNs. Corr, corrected. (Scale bars: 10 μm.) (*B*) Sholl analysis performed in Neurolucida showed that Map1b expression rescued neuritic defects in A53T hNs. Statistical analysis was performed using the area under the curve. Data represent mean ± SEM. **$P < 0.01$ by multiple analysis of variance (MANOVA) and post hoc Tukey test ($n = 50$ individual neurons). n.s., not significant. (*C*) Total dendritic length was also assessed by Sholl analysis. **$P < 0.01$ by MANOVA and post hoc Tukey test. ($n = 50$ individual neurons). *SNCA*-A53T and control hNs of hiPSC (*D*) and hESC (*E*) origin overexpressing Map1b were assessed for axonal varicosities per neurite length, and quantification is presented. **$P < 0.01$ by MANOVA and post hoc Tukey test ($n = 20$ individual neurons).

work, in addition to that of other groups, highlights the therapeutic potential for DMF in PD. Given that this drug has a track record of safety in the treatment of multiple sclerosis and psoriasis, it is a strong candidate for drug repurposing in the treatment of PD.

Materials and Methods

Extended experimental procedures are described in *SI Appendix, Materials and Methods*.

Reagents. All chemicals were purchased through Sigma–Aldrich, and all cell culture reagents were obtained from Invitrogen, except where indicated.

Complementary DNA Constructs and Expression Vectors. Full-length MAP1B fused to the GFP at the N terminus (MAP1B-GFP) was produced by PCR amplification of mouse MAP1B complementary DNA cloned into the pSVsport vector

and subcloned into pEGFP-C1 (48). pcDNA3-EGFP-C4-Nrf2 and pcDNA3-Myc3-Nrf2 were gifts from Yue Xiong, University of North Carolina, Chapel Hill, NC (Addgene plasmid nos. 21549 and 21555) (49).

Cell Culture. With the exception of the WT BGO1 hESCs, the cell lines used in this study were generated and kindly shared by Rudolf Jaenisch, Whitehead Institute, Boston, MA (14). BGO1 hESCs were derived by BresaGen, Inc. Genotypes of WT/corrected and A53T cell lines were confirmed by restriction digest of genomic DNA, as previously described (14). The hiPSC and hESC cultures were routinely cultured and maintained in our laboratory using a protocol described previously (15). Differentiation of hiPSC and hESC cultures into A9-type DA neurons was also performed as described previously (50). More information is provided in *SI Appendix, Materials and Methods*.

Neurite Analysis. Neurite analysis was performed on replated hPSC-derived neurons at 50–60 d in vitro. Tracing was performed in Neurolucida 360 (MBF Bioscience), and Sholl analysis total neurite length and varicosities per neurite length were calculated by Neurolucida 360. More information is provided in *SI Appendix, Materials and Methods*.

Gene Expression Analysis. Microarray data from untreated *SNCA*-A53T and *SNCA*-corrected hNs ($n = 3$ experiments) were collected previously (15) using the Microarray Gene Expression Platform with Illumina beadchip human-HT-12 v4 (data accessible at the National Center for Biotechnology Information [NCBI] Gene Expression Omnibus [GEO], accession no. GSE46798) (51). To identify consistent changes to gene expression in PD, the *SNCA*-A53T hN differentially expressed genes were queried against curated genomic profiles using Illumina's BaseSpace Correlation Engine software (previously known as NextBio Research) to identify highly correlated PD-associated datasets (52). The gene expression profile of SN from 8 sporadic PD patients (Braak α-syn stages 5 through 6) relative to 8 clinically normal controls (Braak α-syn stage 0) harvested post mortem (NCBI GEO accession no. GSE49036) (53) was selected for further comparison with the *SNCA*-A53T hN differentially expressed genes. Details of data analysis using the BaseSpace Correlation Engine (52), GeneMania (54), and the Database for Annotation, Visualization and Integrated Discovery (DAVID) v6.7 (55, 56) are provided in *SI Appendix, Materials and Methods*.

ChIP Assay. ChIP assays were performed using rabbit IgG or a rabbit anti-Nrf2 antibody (Santa Cruz Biotechnology) as previously described (32). The putative AREs within the *Map1b* enhancer that were amplified for determination of Nrf2 binding can be found in *SI Appendix, Table S1*. Levels of enrichment (n-fold) were calculated using the comparative cycle threshold method. For quantitative ChIP, the PCR assay was performed as described in *SI Appendix, Materials and Methods*.

Luciferase Reporter Gene Assays. Cells were transfected with Lipofectamine 2000 (Invitrogen) in 24-well plates with a Nrf2 reporter (Addgene) along with Renilla luciferase control vector or lentivirally infected with the same reporters. Cells were harvested and analyzed using a Dual-Glo Luciferase Assay kit (Promega) following the manufacturer's instructions. Firefly luciferase activity was normalized to Renilla luciferase activity.

Immunocytochemistry and Fluorescence Analysis. Cells were fixed with 4% paraformaldehyde for 20 min, washed once with phosphate-buffered saline (PBS), and blocked with 3% bovine serum albumin and 0.3% Triton X-100 in PBS for 30 min. Cells were incubated with primary antibody overnight, and the appropriate Alexa Fluor (488, 594, 647)-conjugated secondary antibodies from Thermo Life Technologies were used at 1:1,000 dilution. For MitoSOX staining of superoxide anion, cells were loaded with 1.25 μM MitoSOX (Thermo-Life Technologies) in media for 15 min at room temperature. Excess dye was washed out with PBS. Cells were then processed as per the manufacturer's protocol for visualization of differential fluorescence intensities. Imaging was performed using an Axio-Observer microscope with light-emitting diode–based illumination and optical sectioning by structured illumination (Zeiss). Objectives used were plan-apochromat (APO) 40×/1.4 oil differential interference contrast (DIC) visible-infrared or plan-APO 63×/1.4 oil DIC M27.

Protein Immunoprecipitation. For immunoprecipitation assays, protein lysate from hiPSC- or hESC-derived neurons, was precleared overnight with Dynabeads. Protease and phosphatase inhibitors (NaF, phenylmethylsulfonyl fluoride, NaV, and aprotinin) were added to lysis buffers just before use. Protein concentration was determined using the Bio-Rad DC Protein assay. Samples were subsequently incubated with Dyna Protein G magnetic beads (Invitrogen)

Czaniecki et al.

www.manaraa.com

conjugated to α-syn (BD Bioscience) or mouse-IgG (Santa Cruz Biotechnology) antibody. Samples were subsequently centrifuged or placed on a magnetic rack where appropriate. Proteins were eluted in either elution buffer (50 mM glycine, pH 2.8) or boiled and subjected to sodium dodecyl sulfate/polyacrylamide gel electrophoresis (SDS/PAGE). Samples were then processed in the same manner as for Western blots of whole-cell lysate.

Western Blot Analysis. Briefly, samples were separated on a 4 to 12% gradient Bis-Tris SDS/PAGE gel and transferred onto 0.2 μm of nitrocellulose. Membranes probed with primary antibodies were used at a dilution of 1:1,000. When donkey anti-mouse (1:2,000; BioRad) and anti-rabbit (1:2,000; BioRad) horseradish peroxidase-conjugated secondary antibodies were used, clarity

Western enhanced chemiluminescence blotting substrate (Bio-Rad) was used to visualize bands on blots. When anti-mouse (800) and anti-rabbit (700) Li-Cor infrared-conjugated secondary antibodies were used (1:5,000), bands were visualized on the Li-Cor Fc imaging platform. Densitometry was performed to quantify band intensity using the Li-Cor Fc program. Further details can be found in *SI Appendix, Materials and Methods*.

1. W. Dauer, S. Przedborski, Parkinson's disease: Mechanisms and models. *Neuron* **39**, 889–909 (2003).
2. P. J. Spira, D. M. Sharpe, G. Halliday, J. Cavanagh, G. A. Nicholson, Clinical and pathological features of a Parkinsonian syndrome in a family with an Ala53Thr alpha-synuclein mutation. *Ann. Neurol.* **49**, 313–319 (2001).
3. L. J. Martin, S. Semenkow, A. Hanaford, M. Wong, Mitochondrial permeability transition pore regulates Parkinson's disease development in mutant α-synuclein transgenic mice. *Neurobiol. Aging* **35**, 1132–1152 (2014).
4. S. Chandra, G. Gallardo, R. Fernández-Chacón, O. M. Schlüter, T. C. Südhof, Alpha-synuclein cooperates with CSPalpha in preventing neurodegeneration. *Cell* **123**, 383–396 (2005).
5. L. A. Volpicelli-Daley, K. C. Luk, V. M. Lee, Addition of exogenous α-synuclein preformed fibrils to primary neuronal cultures to seed recruitment of endogenous α-synuclein to Lewy body and Lewy neurite-like aggregates. *Nat. Protoc.* **9**, 2135–2146 (2014).
6. K. C. Luk *et al.*, Pathological α-synuclein transmission initiates Parkinson-like neurodegeneration in nontransgenic mice. *Science* **338**, 949–953 (2012).
7. J. J. Zarranz *et al.*, The new mutation, E46K, of alpha-synuclein causes Parkinson and Lewy body dementia. *Ann. Neurol.* **55**, 164–173 (2004).
8. W. Matsuda *et al.*, Single nigrostriatal dopaminergic neurons form widely spread and highly dense axonal arborizations in the neostriatum. *J. Neurosci.* **29**, 444–453 (2009).
9. J. Chen, Y. Kanai, N. J. Cowan, N. Hirokawa, Projection domains of MAP2 and tau determine spacings between microtubules in dendrites and axons. *Nature* **360**, 674–677 (1992).
10. L. I. Binder, A. Frankfurter, L. I. Rebhun, The distribution of tau in the mammalian central nervous system. *J. Cell Biol.* **101**, 1371–1378 (1985).
11. K. Yamaguchi *et al.*, Abundant neuritic inclusions and microvacuolar changes in a case of diffuse Lewy body disease with the A53T mutation in the alpha-synuclein gene. *Acta Neuropathol.* **110**, 298–305 (2005).
12. P. T. Kotzbauer *et al.*, Fibrillization of alpha-synuclein and tau in familial Parkinson's disease caused by the A53T alpha-synuclein mutation. *Exp. Neurol.* **187**, 279–288 (2004).
13. P. H. Jensen *et al.*, Microtubule-associated protein 1B is a component of cortical Lewy bodies and binds alpha-synuclein filaments. *J. Biol. Chem.* **275**, 21500–21507 (2000).
14. F. Soldner *et al.*, Generation of isogenic pluripotent stem cells differing exclusively at two early onset Parkinson point mutations. *Cell* **146**, 318–331 (2011).
15. S. D. Ryan *et al.*, Isogenic human iPSC Parkinson's model shows nitrosative stress-induced dysfunction in MEF2-PGC1α transcription. *Cell* **155**, 1351–1364 (2013).
16. M. G. Stykel *et al.*, Nitration of microtubules blocks axonal mitochondrial transport in a human pluripotent stem cell model of Parkinson's disease. *FASEB J.* **32**, 5350–5364 (2018).
17. T. Ryan *et al.*, Cardiolipin exposure on the outer mitochondrial membrane modulates α-synuclein. *Nat. Commun.* **9**, 817 (2018).
18. J. E. Duda *et al.*, Concurrence of alpha-synuclein and tau brain pathology in the Contursi kindred. *Acta Neuropathol.* **104**, 7–11 (2002).
19. Y. Li *et al.*, Mutant LRRK2(R1441G) BAC transgenic mice recapitulate cardinal features of Parkinson's disease. *Nat. Neurosci.* **12**, 826–828 (2009).
20. R. A. Linker *et al.*, Fumaric acid esters exert neuroprotective effects in neuroinflammation via activation of the Nrf2 antioxidant pathway. *Brain* **134**, 678–692 (2011).
21. R. A. Linker, A. Haghikia, Dimethyl fumarate in multiple sclerosis: Latest developments, evidence and place in therapy. *Ther. Adv. Chronic Dis.* **7**, 198–207 (2016).
22. S. C. Lu, Glutathione synthesis. *Biochim. Biophys. Acta* **1830**, 3143–3153 (2013).
23. E. Kansanen, S. M. Kuosmanen, H. Leinonen, A. L. Levonen, The Keap1-Nrf2 pathway: Mechanisms of activation and dysregulation in cancer. *Redox Biol.* **1**, 45–49 (2013).
24. H. C. Huang, T. Nguyen, C. B. Pickett, Regulation of the antioxidant response element by protein kinase C-mediated phosphorylation of NF-E2-related factor 2. *Proc. Natl. Acad. Sci. U.S.A.* **97**, 12475–12480 (2000).
25. H. C. Huang, T. Nguyen, C. B. Pickett, Phosphorylation of Nrf2 at Ser-40 by protein kinase C regulates antioxidant response element-mediated transcription. *J. Biol. Chem.* **277**, 42769–42774 (2002).
26. N. Ostrerova *et al.*, alpha-Synuclein shares physical and functional homology with 14-3-3 proteins. *J. Neurosci.* **19**, 5782–5791 (1999).
27. K. Itoh *et al.*, Keap1 represses nuclear activation of antioxidant responsive elements by Nrf2 through binding to the amino-terminal Neh2 domain. *Genes Dev.* **13**, 76–86 (1999).
28. G. Kouroupi *et al.*, Defective synaptic connectivity and axonal neuropathology in a human iPSC-based model of familial Parkinson's disease. *Proc. Natl. Acad. Sci. U.S.A.* **114**, E3679–E3688 (2017).
29. A. Meixner *et al.*, MAP1B is required for axon guidance and is involved in the development of the central and peripheral nervous system. *J. Cell Biol.* **151**, 1169–1178 (2000).
30. X. Wang *et al.*, A polymorphic antioxidant response element links NRF2/sMAF binding to enhanced MAPT expression and reduced risk of Parkinsonian disorders. *Cell Rep.* **15**, 830–842 (2016).
31. D. Liu, I. Fischer, Structural analysis of the proximal region of the microtubule-associated protein 1B promoter. *J. Neurochem.* **69**, 910–919 (1997).
32. B. N. Chorley *et al.*, Identification of novel NRF2-regulated genes by ChIP-Seq: Influence on retinoid X receptor alpha. *Nucleic Acids Res.* **40**, 7416–7429 (2012).
33. R. T. Mulcahy, M. A. Wartman, H. H. Bailey, J. J. Gipp, Constitutive and beta-naphthoflavone-induced expression of the human gamma-glutamylcysteine synthetase heavy subunit gene is regulated by a distal antioxidant response element/TRE sequence. *J. Biol. Chem.* **272**, 7445–7454 (1997).
34. O. Hwang, Role of oxidative stress in Parkinson's disease. *Exp. Neurobiol.* **22**, 11–17 (2013).
35. F. Kamp *et al.*, Inhibition of mitochondrial fusion by α-synuclein is rescued by PINK1, Parkin and DJ-1. *EMBO J.* **29**, 3571–3589 (2010).
36. C. Guardia-Laguarta *et al.*, α-Synuclein is localized to mitochondria-associated ER membranes. *J. Neurosci.* **34**, 249–259 (2014).
37. E. S. Luth, I. G. Stavrovskaya, T. Bartels, B. S. Kristal, D. J. Selkoe, Soluble, prefibrillar α-synuclein oligomers promote complex I-dependent, Ca2+-induced mitochondrial dysfunction. *J. Biol. Chem.* **289**, 21490–21507 (2014).
38. S. M. Heman-Ackah *et al.*, Alpha-synuclein induces the unfolded protein response in Parkinson's disease SNCA triplication iPSC-derived neurons. *Hum. Mol. Genet.* **26**, 4441–4450 (2017).
39. D. F. Lázaro *et al.*, Systematic comparison of the effects of alpha-synuclein mutations on its oligomerization and aggregation. *PLoS Genet.* **10**, e1004741 (2014).
40. L. Lin *et al.*, Molecular features underlying neurodegeneration identified through in vitro modeling of genetically diverse Parkinson's disease patients. *Cell Rep.* **15**, 2411–2426 (2016).
41. Z. Wang *et al.*, DJ-1 can inhibit microtubule associated protein 1 B formed aggregates. *Mol. Neurodegener.* **6**, 38 (2011).
42. S. L. Chan, L. L. Chua, D. C. Angeles, E. K. Tan, MAP1B rescues LRRK2 mutant-mediated cytotoxicity. *Mol. Brain* **7**, 29 (2014).
43. A. Atwan *et al.*, Oral fumaric acid esters for psoriasis. *Cochrane Database Syst. Rev.*, CD010497 (2015).
44. M. Ahuja *et al.*, Distinct Nrf2 signaling mechanisms of fumaric acid esters and their role in neuroprotection against 1-methyl-4-phenyl-1,2,3,6-tetrahydropyridine-induced experimental Parkinson's-like disease. *J. Neurosci.* **36**, 6332–6351 (2016).
45. M. Campolo *et al.*, The neuroprotective effect of dimethyl fumarate in an MPTP-mouse model of Parkinson's disease: Involvement of reactive oxygen species/nuclear factor-κB/nuclear transcription factor related to NF-E2. *Antioxid. Redox Signal.* **27**, 453–471 (2017).
46. I. Lastres-Becker *et al.*, Repurposing the NRF2 activator dimethyl fumarate as therapy against synucleinopathy in Parkinson's disease. *Antioxid. Redox Signal.* **25**, 61–77 (2016).
47. X. Jing *et al.*, Dimethyl fumarate attenuates 6-OHDA-induced neurotoxicity in SH-SY5Y cells and in animal model of Parkinson's disease by enhancing Nrf2 activity. *Neuroscience* **286**, 131–140 (2015).
48. T. M. Scales, S. Lin, M. Kraus, R. G. Goold, P. R. Gordon-Weeks, Nonprimed and DYRK1A-primed GSK3 beta-phosphorylation sites on MAP1B regulate microtubule dynamics in growing axons. *J. Cell Sci.* **122**, 2424–2435 (2009).
49. M. Furukawa, Y. Xiong, BTB protein Keap1 targets antioxidant transcription factor Nrf2 for ubiquitination by the Cullin 3-Roc1 ligase. *Mol. Cell. Biol.* **25**, 162–171 (2005).
50. S. Kriks *et al.*, Dopamine neurons derived from human ES cells efficiently engraft in animal models of Parkinson's disease. *Nature* **480**, 547–551 (2011).
51. R. Edgar, M. Domrachev, A. E. Lash, Gene expression Omnibus: NCBI gene expression and hybridization array data repository. *Nucleic Acids Res.* **30**, 207–210 (2002).
52. I. Kupershmidt *et al.*, Ontology-based meta-analysis of global collections of high-throughput public data. *PLoS One* **5**, e13066 (2010).
53. A. A. Dijkstra *et al.*, Evidence for immune response, axonal dysfunction and reduced endocytosis in the substantia nigra in early stage Parkinson's disease. *PLoS One* **10**, e0128651 (2015).
54. D. Warde-Farley *et al.*, The GeneMANIA prediction server: Biological network integration for gene prioritization and predicting gene function. *Nucleic Acids Res.* **38**, W214–W220 (2010).
55. W. Huang da, B. T. Sherman, R. A. Lempicki, Bioinformatics enrichment tools: Paths toward the comprehensive functional analysis of large gene lists. *Nucleic Acids Res.* **37**, 1–13 (2009).
56. W. Huang da, B. T. Sherman, R. A. Lempicki, Systematic and integrative analysis of large gene lists using DAVID bioinformatics resources. *Nat. Protoc.* **4**, 44–57 (2009).

NEUROSCIENCE

Czaniecki et al.

www.manaraa.com